ACS OMEGA

http://pubs.acs.org/journal/acsodf

Article

Monitoring Cell Plasma Membrane Polarity by a NIR Fluorescence Probe with Unexpected Cell Plasma Membrane-Targeting Ability

Jiaojiao Liu, Mei Liu, Fancheng Meng, Jiajia Lv, Mingyan Yang, Jie Gao, Gang Wei,* Zeli Yuan,* and Hongyu Li*

Cite This: *ACS Omega* 2022, 7, 46891−46899

Read Online

ACCESS | Metrics & More | Article Recommendations | Supporting Information

ABSTRACT: The cell plasma membrane, the natural barrier of a cell, plays critical roles in a mass of cell physiological and pathological processes. Therefore, revealing and monitoring the local status of the cell plasma membrane are of great significance. Herein, using a near-infrared (NIR) fluorescence probe BTCy, microenvironmental polarity in the cell plasma membrane was in situ monitored. BTCy showed sensitive and selective fluorescence decrease response at 706 nm with the increase of polarity as its polarity-responsive D−π−A structure. Most importantly, BTCy showed unexpected cell plasma membrane-targeting ability, probably due to its amphiphilic structure. With BTCy, the distinguishing imaging of cancer and normal cells was done, in which cancer cells exhibited significantly stronger signals due to their lower cell plasma membrane polarity. In addition, with the imaging of BTCy, the ferroptosis process was revealed with no significant cell plasma membrane polarity variation for the first time. Furthermore, BTCy was employed for in vivo imaging of tumor tissue in the 4T1-tumor-bearing mice. The polarity-responsive and cell plasma membrane-targeting properties of BTCy make it a useful tool for monitoring cell plasma membrane polarity variation, providing an efficient and simple method for tumor diagnosis.

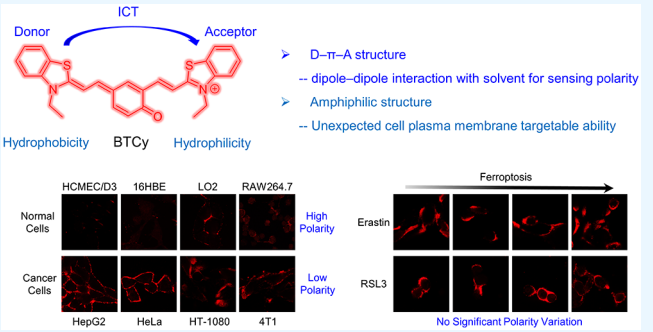

1. INTRODUCTION

The cell plasma membrane, the natural barrier of a cell to isolate and protect its internal microenvironment from the surroundings, plays critical roles in a mass of cell physiological processes, such as the transport of biomolecules and transduction of intercellular signals and immunity,[1−3] and thus, its dysfunction may result in a series of critical diseases.[4−6] As a result, revealing and monitoring the local status of the cell plasma membrane are significant for the early diagnosis of disease, design of new drugs, and modulation of cell signaling. Polarity is one of the most important biological environmental factors in cells. The local polarity of the cell plasma membrane usually reflects the status of its microenvironment, such as variation of lipid composition, lipid peroxidation, interaction of biomolecules, and denaturation or conformational change of membrane proteins.[7−9] Moreover, cancer cells have recently been revealed to have obviously lower cell plasma membrane polarity compared to normal cells.[10,11] This feature of cancer cells is probably employed as a biomarker to distinguish cancer and normal cells. Therefore, the development of an efficient method to monitor cell plasma membrane polarity is urgently needed for the studies of the cell plasma membrane and may also provide a new strategy for the diagnosis of cancer.

Due to their sensitive, high-resolution, and noninvasive analytical properties, fluorescence probes have long been employed for the in situ imaging of bioactive species (e.g., reactive oxygen species, biothiols, and enzymes)[12−15] and cell microenvironmental factors (e.g., pH, viscosity, and polarity)[16−19] in living cells and/or in vivo. Among them, near-infrared (NIR) fluorescence probes with emission in the NIR region (650−900 nm) are much more desirable for bioimaging to avoid biological autofluorescence, increase imaging penetration depth, and reduce light damage.[20,21] Till now, many efforts have been made for the development of fluorescence probes for monitoring biological environmental polarity.[22−31] However, the probes capable of monitoring polarity variation in the cell plasma membrane are still rare,[10,11,32] especially that with fluorescence response in the NIR region.

Herein, a benzothiazole cyanine-based NIR fluorescence probe (BTCy) has been developed for detection of polarity. As shown in Scheme 1, BTCy has a typical polarity-responsive

Received: September 16, 2022
Accepted: November 25, 2022
Published: December 9, 2022

https://doi.org/10.1021/acsomega.2c05997
ACS Omega 2022, 7, 46891−46899

Scheme 1. Structure Design and Response Mechanism of BTCy for Polarity

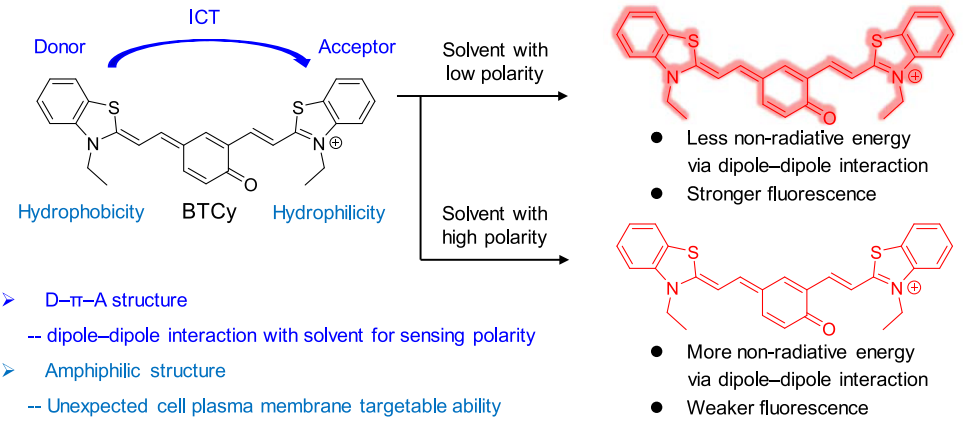

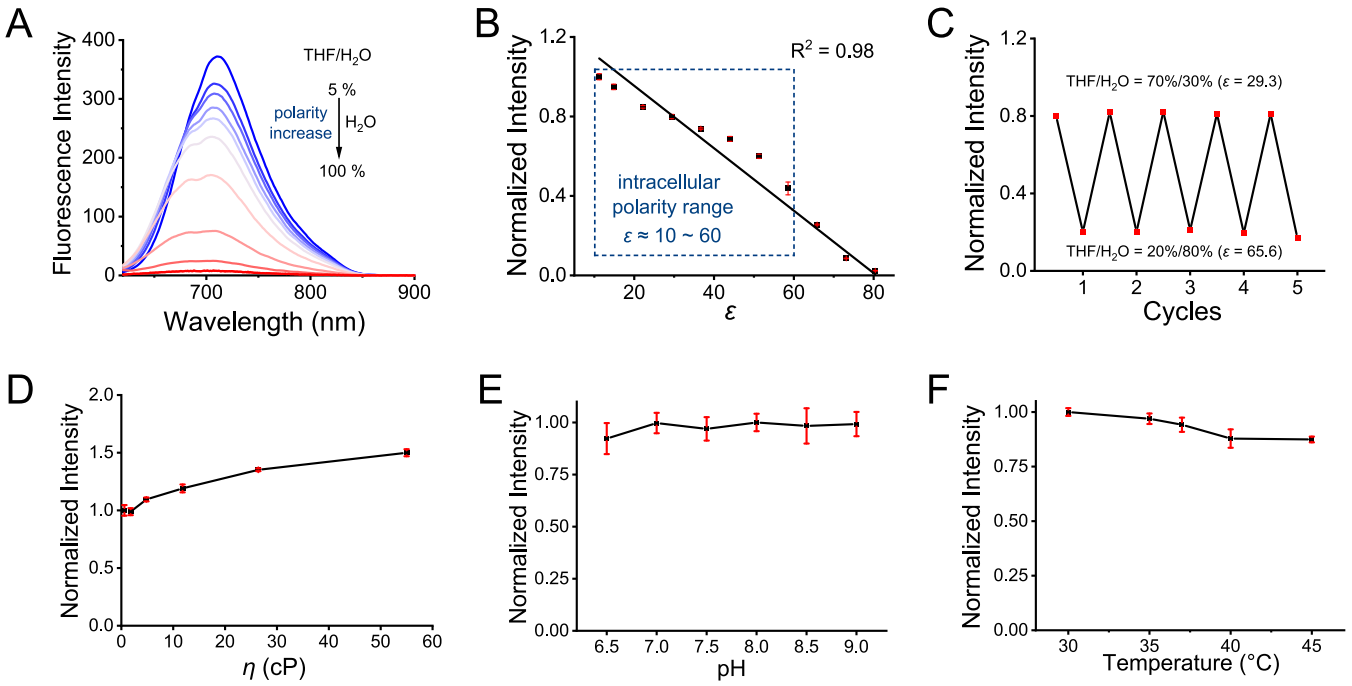

Figure 1. (A) Fluorescence spectra of 10 μM BTCy in THF/H_2O mixtures with different volume proportions. (B) Normalized fluorescence intensity of 10 μM BTCy in THF/H_2O mixtures with dielectric constant (ε) from 11.1 (5% H_2O) to 80.1 (100% H_2O). (C) Reversible cycles of normalized fluorescence intensity in THF/H_2O mixtures with ε = 29.3 (30% H_2O) and 65.6 (80% H_2O). (D) Normalized fluorescence intensity of 10 μM BTCy in MeOH/glycerol mixtures with viscosity (η) from 0.59 cP (0% glycerol) to 55.0 cP (50% glycerol). (E) Normalized fluorescence intensity of 10 μM BTCy in 10 mM phosphate buffer solutions with pH values from 6.5 to 9.0. (F) Normalized fluorescence intensity of 10 μM BTCy in 10 mM phosphate buffer solutions (pH = 7.4) with temperatures from 30 to 45 °C. $\lambda_{ex/em}$ = 610/706 nm.

donor (D)−π−acceptor (A) structure to exhibit an intramolecular charge transfer (ICT) process, which results in the weak fluorescence of the probe in high-polarity solvents due to the strong dipole−dipole interaction between the probes and solvent molecules to dissipate the excited state energy through the nonradiative pathway, whereas strong fluorescence in low-polarity solvents.[30,33] Most of all, despite benzothiazole cyanine-based probes being usually targetable of the cell nucleus or mitochondria,[34−37] BTCy has unexpected cell plasma membrane-targeting ability, which enables the in situ monitoring of polarity in the cell plasm membrane. With the fluorescence imaging of BTCy in cells or in vivo, the distinguishing of cancer and normal cells, imaging of tumor tissue in tumor-bearing mice, and monitoring of cell plasma membrane polarity variation during ferroptosis have been achieved.

2. RESULTS AND DISCUSSION

2.1. Spectral Response of BTCy for Polarity. After BTCy was readily synthesized (Scheme S1) and characterized by ^{1}H NMR, ^{13}C NMR, and HR-MS (Figures S1−S3), its spectral responses to environmental polarity variation were first studied. In this work, environmental polarity was regulated by changing the volume proportions of THF/H_2O mixtures (Table S1), which were commonly employed for testing the analysis properties of the polarity-sensitive probe.[23] As shown in Figure S4, with the increase of solvent polarity from dielectric constant ε = 11.1 to 80.1 (5−100% of H_2O), the absorption peak of BTCy at 637 and 490 nm gradually

https://doi.org/10.1021/acsomega.2c05997
ACS Omega 2022, 7, 46891−46899

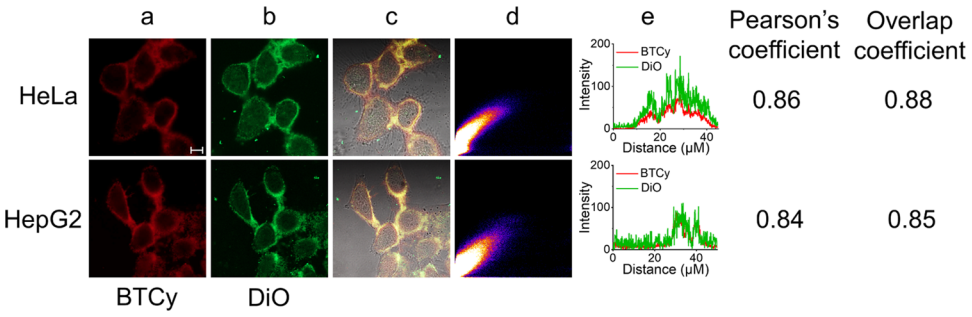

Figure 2. Colocalization imaging of HeLa and HepG2 cells stained with 10 μM BTCy and 10 μM DiO for 30 min. (a) BTCy channel: λ_{ex} = 561 nm, λ_{em} = 600−700 nm. (b) DiO channel: λ_{ex} = 488 nm, λ_{em} = 500−560 nm. (c) Merged image of (a) and (b). (d) Intensity correlation plot of the BTCy channel and the DiO channel. (e) Intensity profiles of BTCy and DiO. Scale bar: 10 μm.

decreased and shifted to 540 and 460 nm, respectively. At the same time, the fluorescence of BTCy at 706 nm presented an about 47-fold decrease (Figure 1A) with the increase of solvent polarity from ε = 11.1 (5% H_2O) to 80.1 (100% H_2O). Importantly, a linear relationship (R^2 = 0.98) between the fluorescence intensity of BTCy and solvent polarity was found from ε = 11.1 to 80.1 (Figure 1B), which covers the intracellular polarity range.[38] There are two possible concerns for the decrease of fluorescence intensity instead of polarity response, one is the aggregation-caused quenching with the increase of H_2O proportion and the other is π-conjugation breaking of BTCy with the addition of H_2O due to the chemical instability and spirocyclization of the dyes with the donor−two-acceptor feature-like BTCy according to the report of Shabat et al.[39] However, the linear increase of fluorescence intensity with BTCy concentration in phosphate buffer solution (Figure S5) indicated that BTCy did not undergo self-aggregation even at a high concentration (50 μM). Furthermore, the absorption spectrum of BTCy in 100% H_2O has two peaks (Figure S4), which is similar to those of NIR donor−two-acceptor dyes in H_2O (e.g., QCy7),[40] suggesting that BTCy presented long π-conjugation in H_2O. Notably, the fluorescence stability of BTCy was also examined, as shown in Figure S6, and the fluorescence of BTCy exhibited satisfying stability whether in dark or under the illumination of a laser lamp, which is comparable to that of the commercial dye cresyl violet. The above finding clearly indicates that in the time scale of the imaging applications (usually tens of minutes to several hours), BTCy exhibits good fluorescence stability, although the chemical instability and spirocyclization may be significant factors that affect the fluorescence property of BTCy. On the other hand, BTCy is reversible to the cyclic variation of polarity between ε = 29.3 (30% H_2O) and 65.6 (80% H_2O) for at least five cycles (Figure 1C), which indicates that BTCy is potentially capable of monitoring the real-time variation of ambient polarity. Besides, the polarity response of BTCy was also tested in 1,4-dioxane/MeOH mixtures (Table S2) or various solvents with varied polarities (Table S3), such as CH_2Cl_2, 1-butanol, EtOH, MeOH, CH_3CN, DMF, and H_2O, which gave similar fluorescence response to that in THF/H_2O (Figures S7 and S8). These results suggested that BTCy is sensitive and suitable for detection of polarity variation.

2.2. Response Selectivity of BTCy for Polarity. To study whether the fluorescence response of BTCy is selective for polarity variation, the fluorescence intensity of BTCy was also tested with the variation of other environmental factors, including viscosity, pH, and temperature. First, the fluorescence response of BTCy to viscosity was tested in MeOH/glycerol mixtures with varied volume proportions (Table S4). It can be seen in Figure 1D that BTCy showed only negligible fluorescence response (about 1.5-fold increase) with the increase of viscosity from η = 0.59 cP (MeOH/glycerol, v/v = 100/0%) to 55.0 cP (MeOH/glycerol, v/v = 50/50%), which is comparable to the intracellular viscosity range.[41] In addition, the fluorescence intensity of BTCy in phosphate buffer solutions was kept almost unaffected with the increase of pH from 6.5 to 9.0 (Figure 1E) and the increase of temperature from 30 to 45 °C (Figure 1F), which covers the physiological pH and temperature. Therefore, other environmental factors would not interfere with the response of BTCy to polarity. Moreover, to exclude the possible response of BTCy to bioactive species, the fluorescence intensities of BTCy in the presence of a series of common bioactive metal ions, amino acids, reactive oxygen species, reductive substances, and anions were tested (Figure S9). The results showed that these tested species could not result in any detectable fluorescence response of BTCy. The above results suggested that BTCy is able to detect the polarity change selectively.

2.3. Fluorescence Imaging of the Cell Plasma Membrane. Due to its sensitive and selective response to polarity, BTCy was employed for monitoring intracellular polarity variation through fluorescence imaging. Before that, the effect of BTCy on cell viability was first investigated by standard MTT assays. As shown in Figure S10, the viabilities of HeLa, HepG2, and HT-1080 cells were still over 85% when treated with 50 μM BTCy for 24 h and close to 100% at a tentative working concentration of 10 μM, indicating that BTCy has low cytotoxicity and is biocompatible for living cells.

Next, colocalization imaging was conducted to investigate the organelle-targeting property of BTCy. HeLa and HepG2 cells were costained with BTCy and commercial organelle dyes (DiO for the cell plasma membrane, LysoTracker Green for lysosomes, and rhodamine 123 for mitochondria). It was found that in either HeLa cells or HepG2 cells, the fluorescence signal from the BTCy channel presented colocalization behavior with that from the DiO channel (Figure 2). However, by contrast, poor colocalization properties were found when the cells were costained with BTCy and the lysosome-targeting dye LysoTracker Green (Figure S11) or mitochondria-targeting dye rhodamine 123 (Figure S12). These results imply the cell plasma membrane-targeting ability of BTCy. As benzothiazole cyanine-based probes in previous reports are usually targetable of the cell nucleus or mitochondria,[34−37] the unexpected cell plasma membrane-targeting ability of BTCy

https://doi.org/10.1021/acsomega.2c05997
ACS Omega 2022, 7, 46891−46899

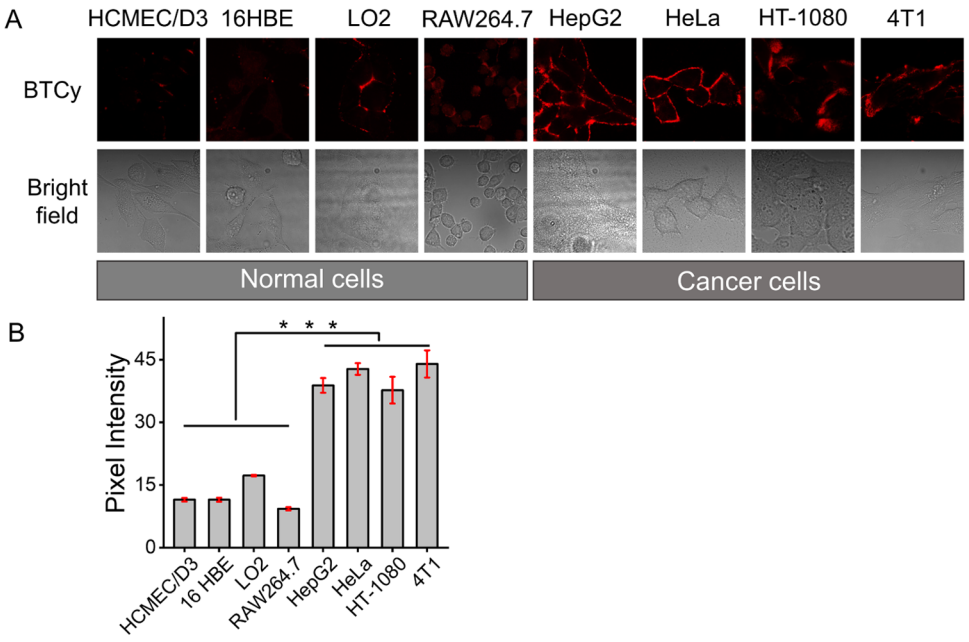

Figure 3. (A) Distinguishing fluorescence imaging of normal cells (HCMEC/D3, 16HBE, LO2, RAW 264.7) and cancer cells (HepG2, HeLa, HT-1080, 4T1) after being stained with BTCy (10 μM) for 30 min. λ_{ex}= 561 nm, λ_{em}= 600−700 nm. (B) Pixel intensities of corresponding fluorescence images from panel (A). The results are presented as mean ± standard deviation (n = 3). A significant difference (***p < 0.001) is performed by Student's t-test.

probably arises from its amphipathic structure feature, which contributes to the retention of the probe in the cell plasma membrane lipid bilayer.[42] Additional experiments were also performed to study the cell plasma membrane-targeting ability of BTCy. As shown in Figure S13, the cell plasma membrane was specifically and strongly lit up after being stained with BTCy for 0.5−5 h; however, in the case of DiO, obvious fluorescence could be detected inside the cells after incubation for 1.5 h, suggesting that BTCy may have better retention in the cell plasma membrane than DiO. In addition, the fluorescence intensity of BTCy on the cell plasma membrane showed slight reduction after 2 h. However, as the staining time for cell imaging in practical applications is usually 10−30 min, BTCy is still capable of specific and efficient imaging of the cell plasma membrane.

Furthermore, the imaging performance of BTCy for the cell plasma membrane was studied. As shown in Figure S14, when HeLa cells were stained with a series of concentrations of BTCy (0.1, 0.5, 1, 5, and 10 μM) for 30 min for imaging, specific fluorescence signals were observed on the cell plasma membrane even at a low concentration at 100 nM, indicating the efficient imaging of the cell plasma membrane by BTCy. Moreover, rapid staining and imaging could be achieved within minutes when HeLa cells were incubated with 10 μM BTCy for 5−30 min (image (a)−(d) of Figure S15). In addition, due to the dim fluorescence of BTCy in the aqueous culture medium, compared with the cells without washing, the fluorescence signal had no obvious change after the cells were incubated with 10 μM BTCy for 30 min and then washed for imaging (Figure S15e), suggesting that BTCy is capable of wash-free imaging of the cell plasma membrane.

2.4. Distinguishing Fluorescence Imaging of Normal and Cancer Cells. Due to its selective response for polarity, as well as rapid and wash-free imaging performance for the cell plasma membrane, BTCy was then employed for the imaging of normal and cancer cells, which were reported to have different cell plasma membrane polarity levels,[10,11] thereby offering a new approach to distinguish normal and cancer cells. Herein, four normal cell lines (HCMEC/D3, 16HBE, LO2, RAW 264.7) and four cancer cell lines (HepG2, HeLa, HT-1080, 4T1) were incubated with 10 μM BTCy for 30 min for imaging. It can be seen from Figure 3 that the fluorescence signals from cancer cells were significantly stronger than those from normal cells. These observations indicate that cancer cells have lower cell plasma membrane polarity than normal cells, which is consistent with the previous report.[10,11] To further study the distinguishing ability of BTCy for normal and cancer cells, RAW 264.7 and HeLa cells (with obvious morphological differences) were cocultured in a cell culture plate and stained with BTCy for imaging. As shown in Figure S16, HeLa cells (larger, fusiform) showed an obviously stronger fluorescence signal (2.7-fold) than RAW 254.7 cells (smaller, round). The above results clearly suggest that BTCy can act as a useful imaging tool for monitoring the cell plasma membrane polarity difference and distinguishing normal and cancer cells.

2.5. Monitoring of Cell Plasma Membrane Polarity Variation during the Ferroptosis Process. The cell plasma membrane is one of the main lipid membrane components of a cell. In the lipid membrane, the local polarity is greatly dependent on lipid organization, such as lipid peroxidation.[7,8] Recently, ferroptosis, an iron-dependent form of cell-programmed death accompanied by significant lipid peroxidation, has attracted great research interest due to its potential physiological and pathological roles.[43,44] Several reports have revealed the increased polarity in lipid droplets during ferroptosis with the utilization of the lipid droplet-targeting polarity fluorescence probe.[26,45] However, it remains unclear whether lipid peroxidation during ferroptosis alters the cell plasma membrane polarity. Therefore, BTCy was applied for monitoring the cell plasma membrane polarity change during ferroptosis to figure out how cell plasma membrane polarity changed in this process and, in addition, verify the

https://doi.org/10.1021/acsomega.2c05997
ACS Omega 2022, 7, 46891−46899

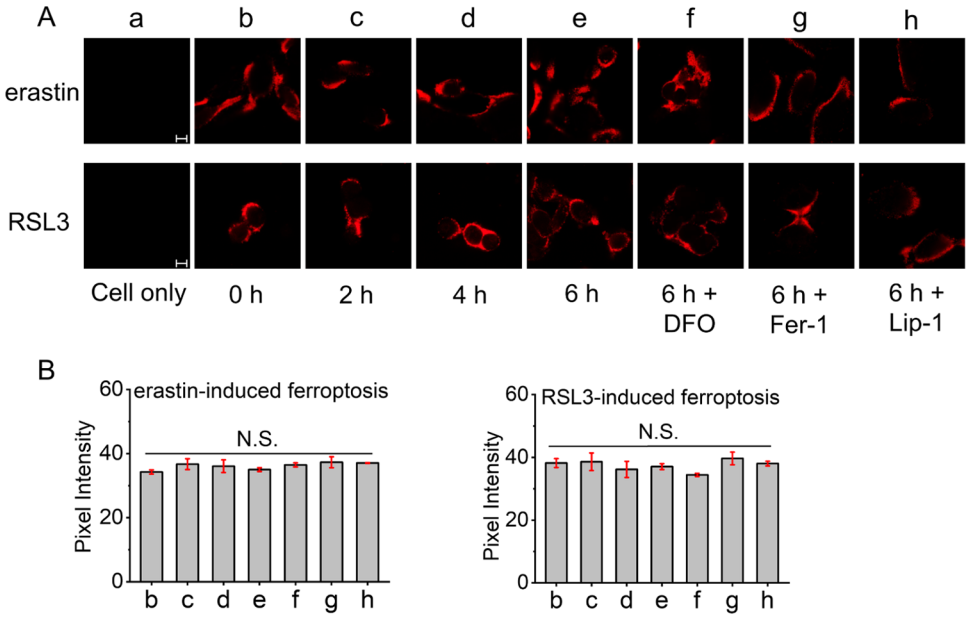

Figure 4. (A) Fluorescence imaging of HT-1080 cells during ferroptosis. (a) Cells only. (b–e) Cells pretreated with 10 μM erastin or 2 μM RSL3 for (b) 0 h, (c) 2 h, (d) 4 h, or (e) 6 h and then stained with 10 μM BTCy for 30 min. (f–h) Cells pretreated with 10 μM erastin or 2 μM RSL3 in the presence of (f) 100 μM DFO, (g) 10 μM Fer-1, or (h) 10 μM Lip-1 for 6 h and then stained with 10 μM BTCy for 30 min. λ_{ex}= 561 nm, λ_{em}= 600–700 nm. Scale bar: 10 μm. (B) Pixel intensities of corresponding fluorescence images from panel (A). The results are presented as mean ± standard deviation (n = 3). A significant difference (N.S., no significance) is performed by Student's t-test.

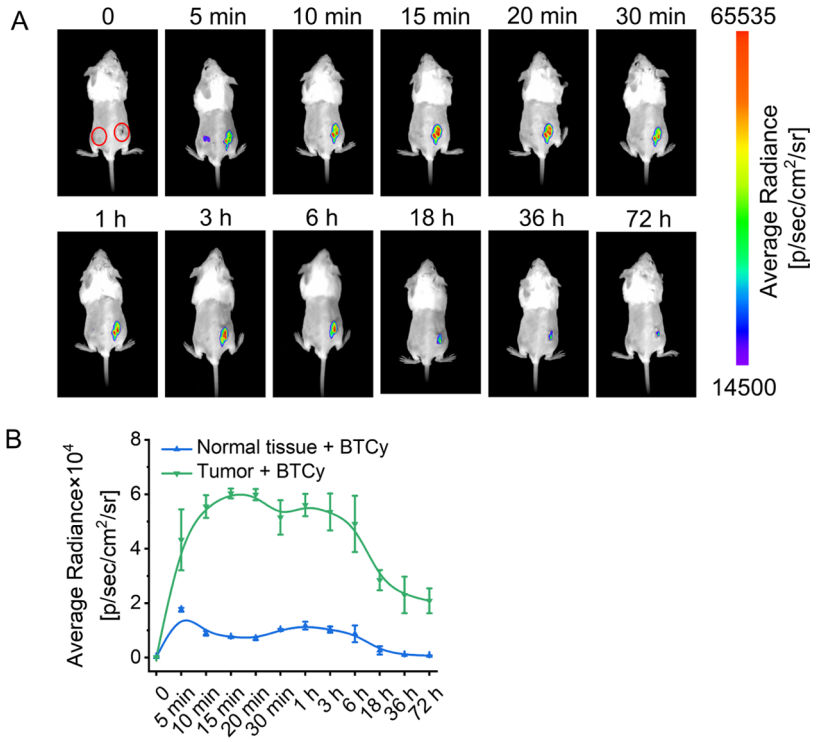

Figure 5. (A) In vivo imaging of the ectopic 4T1 tumor and normal tissue after injection with 25 μL BTCy (0.5 mg/mL in pH 7.4 PBS). (B) Fluorescence intensities from the ectopic 4T1 tumor and normal tissue. The results are presented as mean ± standard deviation (n = 3).

practicability of BTCy. Herein, the commonly used ferroptosis-susceptive HT-1080 cells were treated with the ferroptosis inducer erastin or RSL3 to initiate ferroptosis[44] and then stained with BTCy for fluorescence imaging. As shown in Figure 4, compared with the untreated cells (image (b) of Figure 4A), the fluorescence signals from HT-1080 cells incubated with either erastin or RSL3 for 2–6 h (image (c)–(e) of Figure 4A) had no obvious change. As well, the coincubation with the ferroptosis inhibitor deferoxamine (DFO), Fer-1, or Lip-1[44] did not induce any fluorescence intensity change (image (f)–(h) of Figure 4A). These results suggest that no significant polarity variation occurs in the cell plasma membrane during ferroptosis, despite the disparate initiation mechanisms of the ferroptosis inducer erastin and

https://doi.org/10.1021/acsomega.2c05997
ACS Omega 2022, 7, 46891–46899

RSL3 (the former blocks cystine uptake and depletes intracellular glutathione, and the latter covalently inhibits glutathione peroxidase 4; both eventually lead to accumulation of lipid peroxides and execution of ferroptosis).[44] This finding is quite different from that in lipid droplets, in which the polarity increase is observed during either erastin- or RSL3-induced ferroptosis. This difference may also imply that lipid peroxidation during ferroptosis mainly takes place inside the cell and hardly affects the cell plasma membrane.

2.6. Distinguishing Imaging of Normal and Tumor Tissues. Taking advantage of its NIR fluorescence property, BTCy was next employed for in vivo imaging of normal and tumor tissues. In this experiment, SPF-level BALB/c female mice were chosen to develop an ectopic 4T1 tumor model. BTCy was injected into the tumor area on the right back as well as the normal tissue on the left back. Fluorescence imaging was conducted after injection for the indicated time. As shown in Figure 5, after injection for 5 min, an obvious fluorescence signal was observed in the tumor area. By contrast, a rather weak fluorescence signal was observed in the normal tissue. This difference in fluorescence signals indicated lower polarity in tumors than that in normal tissue, which is consistent with the previously reported observation.[10] In addition, the fluorescence signal from the normal tissue exhibited a rapid decrease. No visible fluorescence signal could be detected in normal tissue after injection for only 10 min. However, the fluorescence signal from the tumor could remain constant for at least 6 h and detectable for at least 72 h. Besides, no detectable fluorescence signal was found in the imaging of the blank tumor and normal tissue injected with PBS (Figure S17), implying the extremely low background fluorescence signal. The above findings clearly indicated that BTCy is capable of rapid and long-time NIR fluorescence imaging of tumors, which would provide an efficient and simple method for tumor diagnosis. The biodistribution of BTCy was also studied after injection in a series of post-injection time points. As shown in Figure S18, after injection for 0.5 h, obvious fluorescence was observed in the tumor and the kidney, which gradually reduced after 6 or 36 h. In addition, a weak fluorescence signal was seen in the liver after 36 h. These observations suggested that BTCy could be excreted rapidly by the kidney and the liver, implying its biosafety.

3. CONCLUSIONS

In summary, we designed and prepared a NIR fluorescence probe BTCy for monitoring cell microenvironmental polarity variation. Due to its D−π−A structure feature, BTCy exhibited sensitive and selective fluorescence decrease response at 706 nm with the increase of polarity, unaffected by other environmental factors, including pH, viscosity, and temperature. Colocalization imaging with the commercial cell plasma membrane dye DiO revealed that BTCy had unexpected cell plasma membrane-targeting ability, which probably resulted from its amphiphilic molecule structure. BTCy was capable of efficient, rapid, and wash-free imaging of the cell plasma membrane. BTCy was then employed for distinguishing imaging of cancer and normal cells, of which the former had lower cell plasma membrane polarity and thus showed an obviously stronger fluorescence signal than the latter. In addition, with the imaging of BTCy, the ferroptosis process was revealed with no significant cell plasma membrane polarity variation for the first time. BTCy was further employed for in vivo imaging of the tumor and normal tissue in the 4T1-tumor-bearing mice, which presented a significantly strong and long-time sustained fluorescence signal in the tumor area compared with the normal tissue. These results clearly indicated that BTCy could act as a useful tool for monitoring cell plasma membrane polarity variation and may provide an efficient and simple method for tumor diagnosis.

4. MATERIALS AND METHODS

4.1. Materials and Instruments. 2-Methylbenzothiazole, 4-hydroxyisophthalaldehyde, rhodamine 123, and 1,4-dioxane were purchased from Energy Chemical (China). LysoTracker Green was purchased from Beyotime Biotechnology Co., Ltd. (Shanghai, China). Thiazolyl blue tetrazolium bromide (MTT) was purchased from Biosharp. Erastin and (1*S*, 3*R*)-RSL3 (RSL3) were obtained from Target Molecule. Dulbecco's modified Eagle medium (DMEM) and fetal bovine serum (FBS) were purchased from Gibco Life Technologies. Trypsin and DiO were obtained from Beijing Solarbio Science & Technology Co., Ltd. Newborn calf serum was purchased from Zhejiang Tianhang Biological Technology Co., Ltd. RPMI 1640 media were purchased from KeyGEN BioTECH Co., Ltd.

NMR spectra were recorded on an Agilent DD2 400 MHz spectrometer. High-resolution mass spectra (HR-MS) were obtained using an Agilent 6550 Q-TOF instrument. UV−vis absorption spectra were performed on a TU-1901 spectrophotometer (Beijing, China). Fluorescence spectra were recorded on a Cary Eclipse fluorescence spectrophotometer (Varian). The MTT assay was measured by a WD-2102B microplate reader (Liuyi, Beijing, China). Fluorescence images were carried out on an LSM 900 confocal laser scanning microscope (CarlZeiss, Germany) with a 63× oil-immersion objective lens and processed with ZEN software or ImageJ software. Mice imaging was performed on a Nightowl LB 983 imaging system (Berthold, Germany).

4.2. Synthesis and Characterization of BTCy. The synthetic route of BTCy is shown in Scheme S1.

First, 1.49 g of 2-methylbenzothiazole (**1**, 10 mmol) and 1.08 g of bromoethane (10 mmol) were reacted in a microwave reactor for 1 h (120 °C, 150 W). The reaction mixture was added with 10 mL of CH_2Cl_2 to form a gray precipitate of 3-ethyl-2-methylbenzo[*d*]thiazol-3-ium bromide (**2**), which was used directly in the next step.

Then, 258 mg of **2** (1 mmol) and 75 mg of 4-hydroxyisophthalaldehyde (**3**, 0.5 mmol) were dissolved in 15 mL methanol with 0.5 mL of pyridine. The mixture was stirred at 65 °C for 12 h. After that, the mixture was cooled down, and the solvent was vapored under reduced pressure. The residue was purified by silica gel column chromatography (CH_2Cl_2/MeOH, 25:1, v/v) to give BTCy as a green powder (120 mg, 51% yield). ^{1}H NMR (400 MHz, 298K, CD_3OD): δ 7.95−7.88 (m, 2H), 7.81−7.75 (m, 5H), 7.65−7.58 (m, 2H), 7.49−7.46 (m, 3H), 7.24−7.20 (m, 1H), 6.94 (d, 1H, J = 16 Hz), 6.36 (d, 1H, J = 8 Hz), 4.59 (d, 4H, J = 4 Hz), 1.48 (d, 6H, J = 8 Hz). ^{13}C NMR (100 MHz, 298K, CD_3OD): δ 180.3, 171.7, 169.8, 169.8, 150.6, 150.5, 148.5, 140.6, 140.6, 128.9, 128.6, 127.4, 127.2, 126.9, 126.6, 124.9, 123.3, 123.3, 123.0, 119.9, 119.9, 114.9, 114.5, 102.6, 43.8, 43.3, 12.7, 12.6. HR-ESI-MS: m/z calcd for BTCy ($C_{28}H_{25}N_2OS_2^+$, $[M]^+$), 469.1403; found, 469.1415.

4.3. Spectral Measurements. BTCy was prepared as a 1 mM stock solution in DMSO. For testing the spectral response

https://doi.org/10.1021/acsomega.2c05997
ACS Omega 2022, 7, 46891−46899

of BTCy to polarity, the BTCy stock solution was diluted to 10 μM by THF/H_2O mixtures and 1,4-dioxane/MeOH mixtures of varied volume proportions, or by various solvents with varied polarities (CH_2Cl_2, 1-butanol, EtOH, MeOH, CH_3CN, DMF, and H_2O). For testing the spectral response of BTCy to viscosity, the BTCy stock solution was diluted to 10 μM by MeOH/glycerol mixtures of varied volume proportions and shaken under 37 °C for 1 h for full mixing. The resulting solutions were stood at room temperature for 30 min for absorption and fluorescence spectra measurements.

4.4. Cells Culture. HT-1080 cells (human fibrosarcoma cells) and 16HBE cells (human bronchial epithelial cells) were planted in RPMI 1640 medium containing 10% (v/v) newborn calf serum, 100 units/mL penicillin and 100 μg/mL streptomycin. HeLa cells (human cervical cancer cells), HCMEC/D3 cells (human brain microvascular endothelial cells), 4T1 cells (mouse breast cancer cells), LO2 cells (human normal hepatocytes), and HepG2 cells (human liver cancer cells) were cultured in DMEM containing 10% (v/v) fetal bovine serum, 100 units/mL penicillin, and 100 μg/mL streptomycin. RAW 264.7 cells (mouse monocyte macrophage) were cultured in RPMI 1640 medium (P/S) and 10% (v/v) heat-inactivated newborn calf serum. All the cells were cultured in a cell incubator under an atmosphere of 5% CO_2 and 95% air with a humidity of 96% and a constant temperature of 37 °C. After growing to 70% density, the cells were treated with trypsin and then planted in glass-bottom dishes for 48 h for further experiments.

4.5. Fluorescence Imaging of Cells. *4.5.1. Colocalization Imaging.* HeLa and HepG2 cells were cultured in glass-bottom dishes for 48 h, then washed with serum-free medium, and finally stained with 10 μM DiO (commercial cell plasma membrane dye), 100 nM LysoTracker Green (commercial lysosome dye), or rhodamine 123 (commercial mitochondria dye) in the presence of 10 μM BTCy for 30 min for fluorescence imaging. The fluorescence imaging of the commercial dye channel was performed with a 488 nm laser as an excitation source and collected fluorescence emission from 500 to 560 nm. The fluorescence imaging of the BTCy channel was performed with a 561 nm laser and collected fluorescence emission from 600 to 700 nm.

4.5.2. Distinguishing Imaging of Normal and Cancer Cells. Normal cells (HCMEC/D3, 16HBE, LO2, and RAW 264.7) or cancer cells (HepG2, HeLa, HT-1080, 4T1) were severally cultured in glass-bottom dishes for 48 h, then washed, and finally stained with 10 μM BTCy for 30 min. Besides, HeLa and RAW 264.7 cells were seeded in the same glass-bottom dish and cocultured for 48 h, then washed, and finally stained with 10 μM BTCy for 30 min. Fluorescence imaging was performed as the above BTCy channel.

4.5.3. Imaging of the Ferroptosis Process. HT-1080 cells were cultured in glass-bottom dishes for 48 h and then incubated with 10 μM erastin or 2 μM RSL3 for the indicated time (2, 4, 6 h). After that, the cells were washed with serum-free medium and stained with 10 μM BTCy for 30 min for fluorescence imaging.

4.6. Imaging of Mice Tumor Model. Five-week-old SPF-level BALB/c female mice were chosen to develop an ectopic tumor model. All animal experiments were approved by the experimental animal ethics committee of Zunyi medical university. The mice were adaptively fed under 25 °C and 40−60% humidity for a week. Then, the back of each mouse was shaved and subcutaneously injected with 100 μL of 4T1 cells (1×10^7 cells/mL in PBS) on the right back. The ectopic 4T1 tumors were allowed to grow to about a size of 100 mm^3. Next, 25 μL of BTCy (0.5 mg/mL in pH 7.4 PBS) was in situ injected into the tumor area, as well as the normal tissue on the left back (control). The in vivo fluorescence imaging of 4T1-tumor-bearing mice was performed with an excitation filter of 620 ± 10 nm and an emission filter of 720 ± 20 nm. In the blank group, 25 μL of PBS was injected into the right 4T1 tumor and left normal tissue of 4T1-tumor-bearing mice for imaging.

■ ASSOCIATED CONTENT

Supporting Information

The Supporting Information is available free of charge at https://pubs.acs.org/doi/10.1021/acsomega.2c05997.

Additional spectra (absorption, fluorescence, NMR, and HR-MS); tables; and fluorescence images (PDF)

■ AUTHOR INFORMATION

Corresponding Authors

Gang Wei − *Commonwealth Scientific and Industrial Research Organization Manufacturing, Lindfield, New South Wales 2070, Australia*; Email: Gang.Wei@csiro.au

Zeli Yuan − *College of Pharmacy, Zunyi Medical University, Zunyi 563003 Guizhou, China; Key Laboratory of Basic Pharmacology of Ministry of Education and Joint International Research Laboratory of Ethnomedicine of Ministry of Education, Zunyi Medical University, Zunyi 563000 Guizhou, China; Guizhou International Scientific and Technological Cooperation Base for Medical Photo-Theranostics Technology and Innovative Drug Development, Zunyi 563003 Guizhou, China;* orcid.org/0000-0001-5354-769X; Email: zlyuan@zmu.edu.cn

Hongyu Li − *College of Pharmacy, Zunyi Medical University, Zunyi 563003 Guizhou, China; Key Laboratory of Basic Pharmacology of Ministry of Education and Joint International Research Laboratory of Ethnomedicine of Ministry of Education, Zunyi Medical University, Zunyi 563000 Guizhou, China; Guizhou International Scientific and Technological Cooperation Base for Medical Photo-Theranostics Technology and Innovative Drug Development, Zunyi 563003 Guizhou, China;* orcid.org/0000-0001-7359-678X; Email: lihongyu@iccas.ac.cn

Authors

Jiaojiao Liu − *College of Pharmacy, Zunyi Medical University, Zunyi 563003 Guizhou, China; Key Laboratory of Basic Pharmacology of Ministry of Education and Joint International Research Laboratory of Ethnomedicine of Ministry of Education, Zunyi Medical University, Zunyi 563000 Guizhou, China; Guizhou International Scientific and Technological Cooperation Base for Medical Photo-Theranostics Technology and Innovative Drug Development, Zunyi 563003 Guizhou, China*

Mei Liu − *College of Pharmacy, Zunyi Medical University, Zunyi 563003 Guizhou, China; Key Laboratory of Basic Pharmacology of Ministry of Education and Joint International Research Laboratory of Ethnomedicine of Ministry of Education, Zunyi Medical University, Zunyi 563000 Guizhou, China; Guizhou International Scientific and Technological Cooperation Base for Medical Photo-*

https://doi.org/10.1021/acsomega.2c05997
ACS Omega 2022, 7, 46891−46899

Theranostics Technology and Innovative Drug Development, Zunyi 563003 Guizhou, China

Fancheng Meng − *College of Pharmacy, Zunyi Medical University, Zunyi 563003 Guizhou, China; Key Laboratory of Basic Pharmacology of Ministry of Education and Joint International Research Laboratory of Ethnomedicine of Ministry of Education, Zunyi Medical University, Zunyi 563000 Guizhou, China; Guizhou International Scientific and Technological Cooperation Base for Medical Photo-Theranostics Technology and Innovative Drug Development, Zunyi 563003 Guizhou, China*

Jiajia Lv − *College of Pharmacy, Zunyi Medical University, Zunyi 563003 Guizhou, China; Key Laboratory of Basic Pharmacology of Ministry of Education and Joint International Research Laboratory of Ethnomedicine of Ministry of Education, Zunyi Medical University, Zunyi 563000 Guizhou, China; Guizhou International Scientific and Technological Cooperation Base for Medical Photo-Theranostics Technology and Innovative Drug Development, Zunyi 563003 Guizhou, China*

Mingyan Yang − *College of Pharmacy, Zunyi Medical University, Zunyi 563003 Guizhou, China; Key Laboratory of Basic Pharmacology of Ministry of Education and Joint International Research Laboratory of Ethnomedicine of Ministry of Education, Zunyi Medical University, Zunyi 563000 Guizhou, China; Guizhou International Scientific and Technological Cooperation Base for Medical Photo-Theranostics Technology and Innovative Drug Development, Zunyi 563003 Guizhou, China*

Jie Gao − *College of Pharmacy, Zunyi Medical University, Zunyi 563003 Guizhou, China; Key Laboratory of Basic Pharmacology of Ministry of Education and Joint International Research Laboratory of Ethnomedicine of Ministry of Education, Zunyi Medical University, Zunyi 563000 Guizhou, China; Guizhou International Scientific and Technological Cooperation Base for Medical Photo-Theranostics Technology and Innovative Drug Development, Zunyi 563003 Guizhou, China*

Complete contact information is available at: https://pubs.acs.org/10.1021/acsomega.2c05997

Notes

The authors declare no competing financial interest.

■ ACKNOWLEDGMENTS

The authors are grateful for the financial support from the National Natural Science Foundation of China (Grant Nos. 82060626, 22004137, and 22164022), Innovative Group Project of Guizhou Province of Education (KY[2018]024), Guizhou Science and Technology Support Program ([2020] 4Y158), Excellent Youth Scientific and Technological Talents of Guizhou Province (Qiankehe Platform Talents [2021] 5638), Guizhou Science and Technology Foundation (Qiankehe basic-ZK[2021] General 046), Talents of Guizhou Science and Technology Cooperation Platform ([2020]4104), Special Project of Academic New Seedling Cultivation and Innovation Exploration of Zunyi Medical University (Qiankehe Platform Talents [2019]-029), Joint foundation of Zunyi Science and Technology Bureau and Zunyi Medical University (Zunshikehe HZ Zi (2020)62, and Qiankehe Platform Talents [2019]-001).

■ REFERENCES

(1) Simons, K.; Ikonen, E. Functional rafts in cell membranes. *Nature* **1997**, *387*, 569−572.
(2) Suzuki, K. G. N. Lipid rafts generate digital-like signal transduction in cell plasma membranes. *Biotechnol. J.* **2012**, *7*, 753−761.
(3) Banfalvi, G. Biological Membranes. In *Permeability of Biological Membranes*; Springer International Publishing: Cham, 2016; pp 1−71.
(4) Yeagle, P. L. Modulation of membrane function by cholesterol. *Biochimie* **1991**, *73*, 1303−1310.
(5) Tabas, I. Consequences of cellular cholesterol accumulation: basic concepts and physiological implications. *J. Clin. Invest.* **2002**, *110*, 905−911.
(6) Ng, D. P.; Poulsen, B. E.; Deber, C. M. Membrane protein misassembly in disease. *Biochim. Biophys. Acta* **2012**, *1818*, 1115−1122.
(7) Danylchuk, D. I.; Jouard, P. H.; Klymchenko, A. S. Targeted solvatochromic fluorescent probes for imaging lipid order in organelles under oxidative and mechanical stress. *J. Am. Chem. Soc.* **2021**, *143*, 912−924.
(8) Ashoka, A. H.; Ashokkumar, P.; Kovtun, Y. P.; Klymchenko, A. S. Solvatochromic near-infrared probe for polarity mapping of biomembranes and lipid droplets in cells under stress. *J. Phys. Chem. Lett.* **2019**, *10*, 2414−2421.
(9) Xiao, H.; Li, P.; Tang, B. Recent progresses in fluorescent probes for detection of polarity. *Coord. Chem. Rev.* **2021**, *427*, No. 213582.
(10) Feng, S.; Liu, Y.; Li, Q.; Gui, Z.; Feng, G. Two water-soluble and wash-free fluorogenic probes for specific lighting up cancer cell membranes and tumors. *Anal. Chem.* **2022**, *94*, 1601−1607.
(11) Li, Q.; Hong, J.; Feng, S.; Gong, S.; Feng, G. Polarity-sensitive cell membrane probe reveals lower polarity of tumor cell membrane and its application for tumor diagnosis. *Anal. Chem.* **2022**, *94*, 11089−11095.
(12) Wu, X.; Shi, W.; Li, X.; Ma, H. Recognition moieties of small molecular fluorescent probes for bioimaging of enzymes. *Acc. Chem. Res.* **2019**, *52*, 1892−1904.
(13) Yue, Y.; Huo, F.; Yin, C. The Chronological evolution of small organic molecular fluorescent probes for thiols. *Chem. Sci.* **2021**, *12*, 1220−1226.
(14) Jiao, X.; Li, Y.; Niu, J.; Xie, X.; Wang, X.; Tang, B. Small-molecule fluorescent probes for imaging and detection of reactive oxygen, nitrogen, and sulfur species in biological systems. *Anal. Chem.* **2018**, *90*, 533−555.
(15) Ashoka, A. H.; Ali, F.; Tiwari, R.; Kumari, R.; Pramanik, S. K.; Das, A. Recent advances in fluorescent probes for detection of HOCl and HNO. *ACS Omega* **2020**, *5*, 1730−1742.
(16) Zhao, Y.; Shi, W.; Li, X.; Ma, H. Recent advances in fluorescent probes for lipid droplets. *Chem. Commun.* **2022**, *58*, 1495−1509.
(17) Li, H.; Liu, Y.; Li, X.; Li, X.; Ma, H. Design, synthesis and application of a dual-functional fluorescent probe for reactive oxygen species and viscosity. *Spectrochim. Acta, Part A* **2021**, *246*, No. 119059.
(18) Yin, J.; Huang, L.; Wu, L.; Li, J.; James, T. D.; Lin, W. Small molecule based fluorescent chemosensors for imaging the micro-environment within specific cellular regions. *Chem. Soc. Rev.* **2021**, *50*, 12098−12150.
(19) Pal, K.; Dutta, T.; Koner, A. L. An enumerated outlook of intracellular micropolarity using solvatochromic organic fluorescent probes. *ACS Omega* **2021**, *6*, 28−37.
(20) Li, H.; Kim, H.; Xu, F.; Han, J.; Yao, Q.; Wang, J.; Pu, K.; Peng, X.; Yoon, J. Activity-based nir fluorescent probes based on the versatile hemicyanine scaffold: design strategy, biomedical applications, and outlook. *Chem. Soc. Rev.* **2022**, *51*, 1795−1835.
(21) Zeng, Z.; Liew, S. S.; Wei, X.; Pu, K. Hemicyanine-based near-infrared activatable probes for imaging and diagnosis of diseases. *Angew. Chem., Int. Ed.* **2021**, *60*, 26454−26475.
(22) Zhou, Y.; Wu, C.; Wang, X.; Li, P.; Fan, N.; Zhang, W.; Liu, Z.; Zhang, W.; Tang, B. Exploring the changes of peroxisomal polarity in

the liver of mice with nonalcoholic fatty liver disease. *Anal. Chem.* **2021**, *93*, 9609−9620.
(23) Fan, L.; Wang, X.; Ge, J.; Li, F.; Wang, X.; Wang, J.; Shuang, S.; Dong, C. A lysosome-targeting and polarity-specific fluorescent probe for cancer diagnosis. *Chem. Commun.* **2019**, *55*, 4703−4706.
(24) Li, P.; Guo, X.; Bai, X.; Wang, X.; Ding, Q.; Zhang, W.; Zhang, W.; Tang, B. Golgi apparatus polarity indicates depression-like behaviors of mice using in vivo fluorescence imaging. *Anal. Chem.* **2019**, *91*, 3382−3388.
(25) Li, M.; Fan, J.; Li, H.; Du, J.; Long, S.; Peng, X. A ratiometric fluorescence probe for lysosomal polarity. *Biomaterials* **2018**, *164*, 98−105.
(26) Wang, K. N.; Liu, L. Y.; Mao, D.; Xu, S.; Tan, C. P.; Cao, Q.; Mao, Z. W.; Liu, B. A polarity-sensitive ratiometric fluorescence probe for monitoring changes in lipid droplets and nucleus during ferroptosis. *Angew. Chem., Int. Ed.* **2021**, *60*, 15095−15100.
(27) Guo, L.; Tian, M.; Zhang, Z.; Lu, Q.; Liu, Z.; Niu, G.; Yu, X. Simultaneous two-color visualization of lipid droplets and endoplasmic reticulum and their interplay by single fluorescent probes in lambda mode. *J. Am. Chem. Soc.* **2021**, *143*, 3169−3179.
(28) Xiao, H.; Zhang, T.; Dong, Y.; Song, X.; Xing, L.; Zhou, J.; Liu, Y.; Zhuo, S. The photophysical properties and imaging application of a new polarity-sensitive fluorescent probe. *Analyst* **2020**, *145*, 6556−6561.
(29) Li, X.; Li, X.; Ma, H. A near-infrared fluorescent probe reveals decreased mitochondrial polarity during mitophagy. *Chem. Sci.* **2020**, *11*, 1617−1622.
(30) Yin, J.; Peng, M.; Ma, Y.; Guo, R.; Lin, W. rational design of a lipid-droplet-polarity based fluorescent probe for potential cancer diagnosis. *Chem. Commun.* **2018**, *54*, 12093−12096.
(31) Jiménez-Sánchez, A.; Lei, E. K.; Kelley, S. O. A multifunctional chemical probe for the measurement of local micropolarity and microviscosity in mitochondria. *Angew. Chem., Int. Ed.* **2018**, *57*, 8891−8895.
(32) Wang, D.; Su, H.; Kwok, R. T. K.; Hu, X.; Zou, H.; Luo, Q.; Lee, M. M. S.; Xu, W.; Lam, J. W. Y.; Tang, B. Z. Rational design of a water-soluble NIR AIEgen, and its application in ultrafast wash-free cellular imaging and photodynamic cancer cell ablation. *Chem. Sci.* **2018**, *9*, 3685−3693.
(33) Wang, S.; Ren, W. X.; Hou, J. T.; Won, M.; An, J.; Chen, X.; Shu, J.; Kim, J. S. Fluorescence imaging of pathophysiological microenvironments. *Chem. Soc. Rev.* **2021**, *50*, 8887−8902.
(34) Narayanaswamy, N.; Das, S.; Samanta, P. K.; Banu, K.; Sharma, G. P.; Mondal, N.; Dhar, S. K.; Pati, S. K.; Govindaraju, T. Sequence-specific recognition of DNA minor groove by an nir-fluorescence switch-on probe and its potential applications. *Nucleic Acids Res.* **2015**, *43*, 8651−8663.
(35) Sakamoto, T.; Yu, Z.; Otani, Y. Dual-color fluorescence switch-on probe for imaging g-quadruplex and double-stranded DNA in living cells. *Anal. Chem.* **2022**, *94*, 4269−4276.
(36) Abeywickrama, C. S.; Bertman, K. A.; Plescia, C. B.; Stahelin, R. V.; Pang, Y. Structural effect on the cellular selectivity of an NIR-emitting cyanine probe: from lysosome to simultaneous nucleus and mitochondria selectivity with potential for monitoring mitochondria dysfunction in cells. *ACS Appl. Bio Mater.* **2019**, *2*, 5174−5181.
(37) Yin, X.; Cai, Y.; Cai, S.; Jiao, X.; Liu, C.; He, S.; Zeng, X. A deep-red fluorescent molecular rotor based on donor-two-acceptor modular system for imaging mitochondrial viscosity. *RSC Adv.* **2020**, *10*, 30825−30831.
(38) Moran, J. L.; Dingari, N. N.; Garcia, P. A.; Buie, C. R. Numerical study of the effect of soft layer properties on bacterial electroporation. *Bioelectrochemistry* **2018**, *123*, 261−272.
(39) Karton-Lifshin, N.; Albertazzi, L.; Bendikov, M.; Baran, P. S.; Shabat, D. "Donor−two-acceptor" dye design: a distinct gateway to NIR fluorescence. *J. Am. Chem. Soc.* **2012**, *134*, 20412−20420.
(40) Karton-Lifshin, N.; Segal, E.; Omer, L.; Portnoy, M.; Satchi-Fainaro, R.; Shabat, D. A unique paradigm for a turn-on near-infrared cyanine-based probe: noninvasive intravital optical imaging of hydrogen peroxide. *J. Am. Chem. Soc.* **2011**, *133*, 10960−10965.
(41) Kuimova, M. K. Mapping viscosity in cells using molecular rotors. *Phys. Chem. Chem. Phys.* **2012**, *14*, 12671−12686.
(42) Liu, C.; Gao, X.; Yuan, J.; Zhang, R. Advances in the development of fluorescence probes for cell plasma membrane imaging. *TrAC, Trends Anal. Chem.* **2020**, *133*, No. 116092.
(43) Jiang, X.; Stockwell, B. R.; Conrad, M. Ferroptosis: mechanisms, biology and role in disease. *Nat. Rev. Mol. Cell Biol.* **2021**, *22*, 266−282.
(44) Stockwell, B. R.; Angeli, F.; Bayir, J. P.; Bush, H.; Conrad, A. I.; Dixon, M.; Fulda, S. J.; Gascón, S.; Hatzios, S.; Kagan, S. K.; Noel, V. E.; Jiang, K.; Linkermann, X.; Murphy, A.; Overholtzer, M. E.; Oyagi, M.; Pagnussat, A.; Park, G. C.; Ran, J.; Rosenfeld, Q.; Salnikow, C. S.; Tang, K.; Torti, D.; Torti, F. M.; Toyokuni, S. V.; Woerpel, S.; Zhang, D. D. Ferroptosis: a regulated cell death nexus linking metabolism, redox biology, and disease. *Cell* **2017**, *171*, 273−285.
(45) Xie, P.; Liu, J.; Yang, X.; Zhu, W.; Ye, Y. A bifunctional fluorescent probe for imaging lipid droplets polarity/SO2 during ferroptosis. *Sens. Actuators, B* **2022**, *365*, No. 131937.

https://doi.org/10.1021/acsomega.2c05997
ACS Omega 2022, 7, 46891−46899